Kinetic, pharmacological and activity-dependent separation of two Ca2+ signalling pathways mediated by type 1 metabotropic glutamate receptors in rat Purkinje neurones

Marco Canepari and David Ogden

J. Physiol. 2006;573;65-82; originally published online Feb 23, 2006;

DOI: 10.1113/jphysiol.2005.103770

Kinetic, pharmacological and activity-dependent separation of two Ca^{2+} signalling pathways mediated by type 1 metabotropic glutamate receptors in rat Purkinje neurones

Marco Canepari[1] and David Ogden[1,2]

[1] *National Institute for Medical Research, London NW7 1AA, UK*
[2] *Laboratoire de Physiologie Cérébrale UMR8118 Université Paris 5, Paris 75006, France*

Type 1 metabotropic glutamate receptors (mGluR1) in Purkinje neurones (PNs) are important for motor learning and coordination. Here, two divergent mGluR1 Ca^{2+}-signalling pathways and the associated membrane conductances were distinguished kinetically and pharmacologically after activation by 1-ms photorelease of L-glutamate or by bursts of parallel fibre (PF) stimulation. A new, mGluR1-mediated transient K^+ conductance was seen prior to the slow EPSC (sEPSC). It was seen only in PNs previously allowed to fire spontaneously or held at depolarized potentials for several seconds and was slowly inhibited by agatoxin IVA, which blocks P/Q-type Ca^{2+} channels. It peaked in 148 ms, had well-defined kinetics and, unlike the sEPSC, was abolished by the phospholipase C (PLC) inhibitor U73122. It was blocked by the BK Ca^{2+}-activated K^+ channel blocker iberiotoxin and unaffected by apamin, indicating selective activation of BK channels by PLC-dependent store-released Ca^{2+}. The K^+ conductance and underlying transient Ca^{2+} release showed a highly reproducible delay of 99.5 ms following PF burst stimulation, with a precision of 1–2 ms in repeated responses of the same PN, and a subsequent fast rise and fall of Ca^{2+} concentration. Analysis of Ca^{2+} signals showed that activation of the K^+ conductance by Ca^{2+} release occured in small dendrites and subresolution structures, most probably spines. The results show that PF burst stimulation activates two pathways of mGluR1 signalling in PNs. First, transient, PLC-dependent Ca^{2+} release from stores with precisely reproducible timing and second, slower Ca^{2+} influx in the cation-permeable sEPSC channel. The priming by prior Ca^{2+} influx in P/Q-type Ca^{2+} channels may determine the path of mGluR1 signalling. The precise timing of PLC-mediated store release may be important for interactions of PF mGluR1 signalling with other inputs to the PN.

(Resubmitted 22 December 2005; accepted after revision 21 February 2006; first published online 23 February 2006)
Corresponding author D. Ogden: National Institute for Medical Research, Mill Hill, London NW7 1AA, UK.
Email: dogden@nimr.mrc.ac.uk

The type-1 metabotropic glutamate receptorss (mGluR1) are required for cerebellar motor learning and synaptic plasticity in Purkinje neurones (PNs), as evidenced by the ataxia observed in mice deficient in mGluR1α (Conquet *et al.* 1994; Aiba *et al.* 1994; Ichise *et al.* 2000; Kishimoto *et al.* 2002) and the clinical neoplastic cerebellar ataxia induced by autoantibodies generated against mGluR1α (Sillevis-Smitt *et al.* 2000; Coesmans *et al.* 2003). *In vitro*, long-term depression (LTD) of parallel fibre (PF) transmission to PNs, resulting from repeated paired stimulation of PF and climbing fibre (CF) inputs, is thought to generate the plastic changes that underlie learned motor coordination (reviewed by Mauk *et al.* 1998). This form of synaptic plasticity is impaired in mGluR1-deficient mice (Conquet *et al.* 1994; Aiba *et al.* 1994; Ichise *et al.* 2000).

mGluR1 are located in the perisynaptic regions of the PF synapse (Baude *et al.* 1993). Activation by PFs initiates two distinct intracellular pathways: (i) activation of phospholipase C (PLC) leading to an increase in D-*myo*-inositol-1,4,5-trisphosphate (IP_3) (Okubo *et al.* 2004) producing Ca^{2+} release from intracellular stores (Khodakhah & Ogden, 1993; Finch & Augustine, 1998; Takechi *et al.* 1998); and (ii) activation of a slow excitatory postsynaptic potential (sEPSP, Batchelor *et al.* 1994) mediated by a non-selective cation channel (Canepari *et al.* 2001*b*) that is permeable to Ca^{2+} (Canepari *et al.* 2004) and thought to be transient receptor potential type 1

 DOI: 10.1113/jphysiol.2005.103770

(TRPC1; Kim *et al.* 2003). Both pathways require the G-protein G_q (Hartmann *et al.* 2004) but appear to diverge before activation of PLC; the mGluR1 excitatory current is insensitive to inhibition of PLCβ (Canepari & Ogden, 2003). Also, both pathways generate an increase in Ca^{2+} concentration but apparently via different mechanisms (Takechi *et al.* 1998; Canepari *et al.* 2004). The experiments described here distinguish between the two pathways kinetically and pharmacologically and describe properties of fast, PLC-dependent Ca^{2+} signalling which have been shown to underlie a transient K^+ conductance.

The PLC signalling pathway resulting in Ca^{2+} release from stores by IP_3 is of particular interest but has been difficult to demonstrate definitively in electrophysiological experiments in PNs. Experiments using photorelease of IP_3 have shown that Ca^{2+} release has properties that differ substantially from those of Ca^{2+} release in non-neuronal tissues (Khodakhah & Ogden, 1993, 1995; Ogden & Capiod, 1997; Fujiwara *et al.* 2001). Particularly, 50-fold higher concentrations of IP_3 (greater than 10 μM) are required to activate Ca^{2+} release and the kinetics of Ca^{2+} release and Ca^{2+}-dependent inactivation of release are much faster than seen in peripheral tissues. The high concentrations and fast kinetics suggest that PLC signalling in PNs may be adapted to act on the time scale of fast transmission (Khodakhah & Ogden, 1995; Ogden, 1996; Ogden & Capiod, 1997; Fujiwara *et al.* 2001). Ca^{2+} release by photoreleased IP_3 produces a fast, inhibitory Ca^{2+}-activated K^+ conductance with a time course similar to the underlying Ca^{2+} increase (Khodakhah & Ogden, 1995). This contrasts with the electrical response commonly reported following mGluR1 activation, slow EPSC (sEPSC), and there are no reports or evidence from previous experiments of an inhibitory K^+ conductance attributible to IP_3. However, a role of IP_3 in the generation of LTD in PNs has been suggested by the ability of photoreleased IP_3 to substitute for PF stimulation in LTD protocols (Khodakhah & Armstrong, 1997; Daniel *et al.* 1999). Thus, there are two long-standing unresolved issues concerning PF-evoked mGluR1 signalling in PNs via the phosphoinsositide pathway. First, the reason for the apparent absence of an inhibitory conductance due to IP_3-mediated Ca^{2+} release and, second, the role of the fast kinetics and low sensitivity of IP_3-evoked Ca^{2+} release in the physiology of the PN. In the experiments described here, transient activation of a Ca^{2+}-activated BK K^+ conductance is described and shown to monitor the time course of mGluR1-mediated, PLC-dependent Ca^{2+} release in small PN dendrites. The PLC-mediated Ca^{2+} release was not seen in quiescent preparations, requiring prior activity and influx of Ca^{2+}. It had fast kinetics similar to IP_3-evoked Ca^{2+} release previously described and generated a precisely timed pulse of Ca^{2+} in small dendrites and spines following PF burst stimulation. The two mGluR1 signalling pathways, producing either Ca^{2+} release from stores or Ca^{2+} influx through the sEPSP channel, are separated kinetically, pharmacologically and by the requirement for prior activity.

Methods

Slice preparation

Wistar rats (19–24 days old) were killed by cervical dislocation, the brain removed and placed in iced saline and parasagittal (thickness, 200 μm) or coronal (thickness, 300 μm) slices were cut from the cerebellum. Slices were kept for 1 h at 32°C and then at room temperature (20–24°C) in a solution containing (mM): NaCl 125, KCl 4, $MgSO_4$ 2, $CaCl_2$ 2, $NaHCO_3$ 25 and glucose 25; gassed with 5% CO_2–95% O_2. Slices were viewed with a Zeiss Axioskop 1FS (Oberkochen, Germany) with a Leica 63× 0.9w objective (Wetzlar, Germany; 40 × when used at 160 mm in this study) and 550/40-nm band-pass illumination.

Electrophysiology

To minimize consumption of 4-methoxy-7-nitroindolinyl (MNI)-caged L-glutamate, experiments were performed without perfusion in 1 ml solution as previously described (Canepari *et al.* 2001*b*, 2004). The external solution contained (mM): NaCl 135, KCl 4, $MgSO_4$ 2, $CaCl_2$ 2, $NaHCO_3$ 2, glucose 25 and Hepes 10; pH 7.3 and 305 mosmol · kg); a continuous stream of hydrated 99.5% O_2–0.5% CO_2 was blown over the surface of the solution. Experiments were performed at 32°C. To isolate mGluR1 signals, experiments were performed with ionotropic glutamate receptor antagonists 2,3-dioxo-6-nitro-1,2,3,4-tetrahydrobenzo[f]quinoxaline -7-sulphonamide (NBQX, 50–100 μM) and 2-amino-5-phosphonopentanoic acid (AP5, 50 μM), and with $GABA_A$ receptor antagonists bicuculline (20 μM) or picrotoxin (100 μM). Most photolysis experiments were done in the presence of tetrodotoxin (TTX, 1 μM) and the P/Q-type Ca^{2+} channel blocker agatoxin IVA (AGA4A, 250 nM). MNI-caged L-glutamate and drugs were applied in 1 ml static solution. Chemicals were Analar grade (BDH, Poole, UK), and biochemicals and drugs were obtained from Sigma (Poole, UK), Tocris (Bristol, UK) or Research Biochemicals (Poole, UK). Experiments with the Ca^{2+} channel blocker AGA4A (Peptide Institute, Osaka, Japan) or K^+ channel blocker iberiotoxin were done with 0.1 mg ml^{-1} cytochrome c present to avoid non-specific binding. MNI-caged L-glutamate (Papageorgiou *et al.* 1999) was synthesized, purified and kindly provided by John Corrie and George Papageorgiou (National Institute for Medical Research, London, UK). Whole-cell recordings were with an

Axopatch 200A (Axon Instruments, Union City, CA, USA) and 2.5-MΩ pipettes filled with the following internal solution (mM): potassium gluconate 110, Hepes 50, KCl 10, $MgSO_4$ 4, Na_2ATP 4, creatine phosphate 10, GTP 0.05; pH was adjusted to 7.3 with KOH. Potentials were corrected for the junction potential of 12 mV pipette negative between this solution and external solution. Series resistance was monitored at 5-min intervals; in 36 experiments with precise measurement it averaged 11.9 ± 2 MΩ (S.D.,). If the leak current at −77 mV exceeded −0.5 nA, experiments were discontinued.

Photolysis

L-Glutamate release from MNI-caged L-glutamate was with a xenon arc flashlamp (Rapp Optoelektronik) filtered at 290–370 nm (UG11; Schott, Mainz, Germany) and focused by a silica condenser through the slice to illuminate a 200-μm diameter spot on the top surface. Uniform illumination (coefficient of variation (CV) = 4.5%) was shown by photolysis of 1-(2-nitrophenyl)ethylpyranine (NPE-HPTS) in Sylgard vesicles (for methods see Canepari *et al.* 2001*a*) distributed over the field, or by fluorescence of 6-μm beads excited by the flash. L-Glutamate concentrations between 6 and 120 μM were obtained by calibrated photolysis, with neutral-density filters in the photolysis light path, and correction for transmission in the slice as described by Canepari *et al.* (2001*a*, 2004).

Acquisition and analysis

Whole-cell patch-clamp data were sampled at 10 kHz with Spike 2 and a Power 1401 interface (Cambridge Electronic Design, Cambridge, UK) after low-pass filtering at 2 kHz (−3 dB). Data were analysed in Matlab 6 (The Mathworks Inc., Natick, MA, USA) or Igor Pro (Wavemetrics). In some experiments at a holding potential of nominally −12 mV, the effects of loss of voltage clamp on the dendritic potential was assessed from −5-mV pulses applied to the pipette at the beginning of each recording; the evoked current was low-pass filtered at 50 kHz, sampled at 250 kHz and fitted with the predictions of a two-compartment model to estimate the voltage error as described by Canepari *et al.* (2004). In these measurements, 10 μM ZD-7288 was present to block the hyperpolarization-activated current (I_H).

Ca^{2+} imaging

The low-affinity fluorescent indicator Oregon Green BAPTA-5N (900 μM; Molecular Probes, Eugene, OR, USA) was included in the internal solution and experiments were performed 30 min after establishing whole-cell recording. The batch of Oregon Green BAPTA-5N had a K_{Ca} value of 35 μM and ratio of maximum (F_{max}) to minimum fluorescence (F_{min}) F_{max}/F_{min} of 27; these values are close to those reported by DiGregorio & Vergara (1997). Fluorescence epi-illumination at 470 nm from fibre-coupled monochromator was uniform over the field (CV ± 10%) and emission images at 520–650 nm (Semrock Inc., Rochester, NY, USA) were collected by an electron multiplying EM-CCD camera (512 × 512 pixels; Andor, Belfast, UK) mounted on a rotatable *x–y* stage. Images of CCD subregions, usually orientated as strips of 512 pixels × 32 pixels, 512 pixels × 64 pixels or 512 pixels × 128 pixels along the dendritic tree (512 pixels is 155 μm; pixel length, 0.3 μm), were acquired at 50 frames s^{-1} (14 bits) with 18.6-ms exposure time at EM gains above 150. Images were analysed in Matlab 6. The background fluorescence of the slice was averaged from a region of 8 × 8 pixels (2.5 × 2.5 μm) approximately 150 μm from the soma in the molecular layer, outside the dendritic field of the PN. The background fluorescence was subtracted and fluorescence changes, ΔF, in each pixel relative to the average, F, of four frames prior to the flash were calculated as the ratio $\Delta F/F$. Spatial variation of background fluorescence in the peripheral dendritic field was small compared with the fluorescence of dendrites loaded with indicator and will have negligible influence on $\Delta F/F$. The background fluorescence close to the soma was higher due to indicator leakage from the pipette prior to sealing. Calculations show that the effect of using the lower, more distal background described above may be to underestimate the amplitude (but not the signal to noise ratio) of $\Delta F/F$ by up to 50% close to the soma. The increase in free Ca^{2+} concentration ($\Delta[Ca^{2+}]_{free}$) was calculated from the approximate relation:
$\Delta[Ca^{2+}]_{free} = K_{Ca}(\Delta F/F)/(F_{max}/F_{min})$ used for low affinity indicators assuming resting fluorescence F is $\sim F_{min}$ and $F_{max} \gg (\Delta F + F)$. With the measured values of K_{Ca} and F_{max}/F_{min}, a $\Delta F/F$ value of 77% corresponded to a $\Delta[Ca^{2+}]_{free}$ of 1 μM.

Results

Kinetic separation of an mGluR1-mediated K^+ conductance from the mGluR1-mediated sEPSC

Experiments to investigate the voltage dependence of the mGluR1-mediated excitatory conductance in PNs evoked by photorelease of L-glutamate over the PN soma and dendrites showed an unexpected transient outward current in depolarized PNs which preceded the excitatory conductance previously described (Canepari *et al.* 2001*b*, 2004; Canepari & Ogden, 2003). The origin of this current is analysed here. Normally, at −77 mV with AMPA receptors blocked, uniform, 1-ms photorelease of L-glutamate activates a fast, transient inward current, due to electrogenic glutamate transport, followed by a slow inward current corresponding to the sEPSC (Fig. 1*A* left trace; Canepari *et al.* 2001*b*). The glutamate

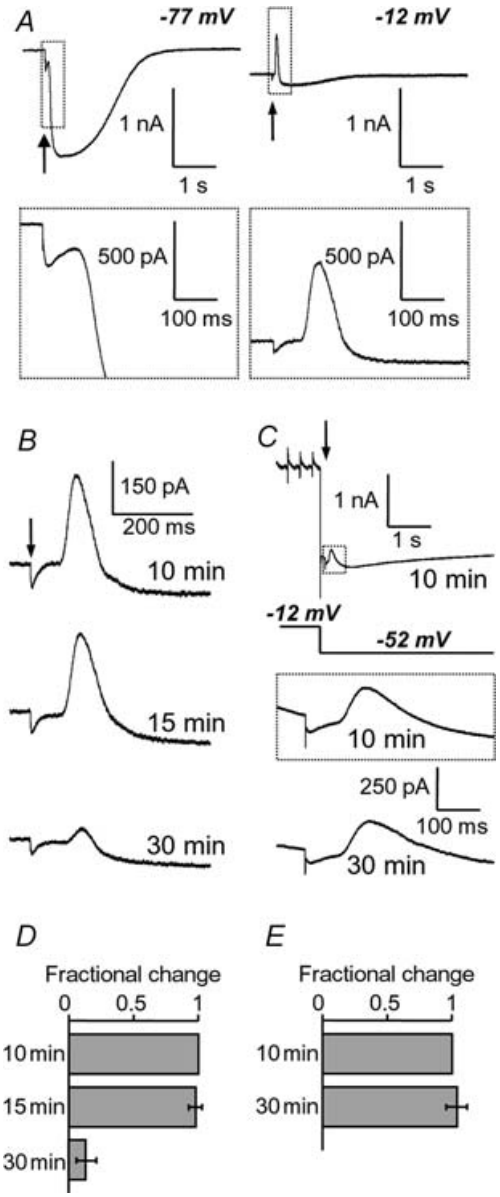

Figure 1. Two mGluR1-mediated membrane currents distinguished by dependence on Ca^{2+} influx
A, mGluR1-mediated currents evoked at −77 mV (left trace) and at −12 mV (right trace) by photorelease of 30 μM L-glutamate at time indicated by arrow. Time scale, 5 s. The regions inside the dotted boxes are shown on time scale of 500 ms below. The initial inward current due to activation of glutamate transporters is seen at both potentials. The late slow inward current is seen most clearly at −77 mV, and the early transient outward current at −12 mV. Note different time scales. *B*, records at −12 mV showing the mGluR1-mediated outward current elicited by photorelease of 30 μM L-glutamate after 10 min (top trace), 15 min (middle trace) and 30 min (bottom trace) incubation in 250 nM AGA4A. Note the run down of the outward current. *C*, top trace, current due to potential step from −12 to −52 mV followed immediately by photorelease of 30 μM L-glutamate. Region indicated by box expanded in bottom traces; same voltage protocol after 10 min and 30 min recording without AGA4A. Note transient outward currents have similar amplitudes at 10 and 30 min. *D*, bar graphs of the outward current amplitudes at −12 mV in the presence of 250 nM AGA4A after 10, 15 and 30 min incubation normalized to amplitudes after 10 min in AGA4A. Data are from six cells. *E*, bar graph of the outward current amplitudes at −45 to −55 mV obtained with the protocol of Fig. 1*C* in the absence of AGA4A. Amplitudes after 10 and 30 min incubation normalized to the amplitude after 10 min. Data are from six cells. In *D* and *E*, error bars indicate the S.E.M. Experiments were done in the presence of 100 μM NBQX, 50 μM AP5, 20 μM bicuculline and 1 μM TTX.

transporter current is seen more clearly in the expanded lower record (Fig. 1*A* lower left). However, at −12 mV pipette potential with excitability suppressed (see below), an additional component of current, a transient outward current activated with a delay of close to 100 ms, precedes the slow inward current. This is shown in the right hand records of Fig. 1*A*. Following the delay, the outward current had rapid kinetics of onset and termination, similar to the K^+ conductance evoked by photorelease of IP_3 mediated by store-released Ca^{2+} seen previously in PNs (Khodakhah & Ogden, 1995). The transient outward current was not seen in previous studies in PNs maintained at −65 to −77 mV with activation of mGluR1 either by photorelease of L-glutamate or by PF stimulation (Canepari *et al.* 2001*b*, 2004; Canepari & Ogden, 2003). It was seen here only after depolarization for 10 s or longer to a pipette potential of −12 mV (estimated to be approximately −33 mV in the peripheral dendritic compartment; see below and Canepari *et al.* 2004). Both mGluR1-mediated currents were also seen with PF stimulation as described below (see Fig. 3). To test which ionic species was carrying the current, the Cl^- equilibrium potential was changed from −67 to −18 mV by increasing internal Cl^- concentration in both photorelease and PF stimulation experiments; this had no effect on the outward current ($n = 5$). K^+ is the only remaining ion with an outwardly directed electrochemical potential gradient, therefore these results suggest high permeability to K^+ but not Cl^-. The signalling pathway, the kinetics and the changes in cytosolic Ca^{2+} concentration underlying the outward current are analysed in the experiments described here.

A role for prior Ca^{2+} entry in the activation of the transient outward current

To prevent fast and slow unclamped spike currents in the soma and dendrites during experiments at −12 mV, TTX (1 μM; to block Na^+ channels) and AGA4A (250 nM; to block P/Q-type Ca^{2+} channels) were applied in the external solution. It was noted that after adding AGA4A to the bath, the size of the early outward current progressively declined most probably due to the progressive block of P/Q-type channels as AGA4A equilibrated slowly in the slice (e.g. Doroshenko *et al.* 1997). In 36 cells, photorelease of L-glutamate at concentrations in the range 6–60 μM evoked outward currents with amplitudes of 100–1000 pA at −12 mV after 10-min incubation in recording solution

containing 250 nM AGA4A, which is sufficient exposure to block Ca^{2+} spikes. However, longer exposures to the recording solution resulted in smaller mGluR1-dependent outward current; the amplitude after 30-min incubation was reduced to 12 ± 4% (S.E.M., $n = 10$) of that recorded after 10-min exposure. The progressive decline of K^+ current in a single cell and a summary of the data from 10 cells are shown in Fig. 1*B* and *D*, respectively. However, controls with the same protocol in the absence of AGA4A were affected by dendritic Ca^{2+} spikes. To overcome this, five control cells were depolarized in the same way but restored to −55 mV just before the flash to test the K^+ current, thus avoiding the contamination with repetitive Ca^{2+} spiking seen at −12 mV in the absence of AGA4A. The data without AGA4A show no decline of the outward current evoked by L-glutamate release after 30 min. These data are summarized in Fig. 1*C* and *E*. Therefore, the decline of outward current may be attributable to the slow onset of AGA4A in blocking Ca^{2+} influx, and indicates a role of Ca^{2+} influx via P/Q-type channels in generating the transient K^+ conductance seen after activation of mGluR1 by photoreleased L-glutamate.

Pharmacological separation of outward and inward currents

The pharmacology of the mGluR1-dependent excitatory conductance has been previously described (Canepari *et al.* 2001*b*, 2004; Canepari & Ogden, 2003) and can be summarized. The slow excitatory mGluR1 conductance underlying the sEPSP of PNs is insensitive to inhibition of PLCβ by the drug U73122, which has been shown to block PLCβ4 (Cruzblanca *et al.* 1998; Haley *et al.* 2000; Horowitz *et al.* 2005) the isoform present in PNs (Sugiyama *et al.* 1999). However, the excitatory current is blocked by pore-blocking ligands of unedited glutamate receptors (GluRs), such as naphthylacetylspermine (NASP) or IEM1460 (Canepari *et al.* 2004). It is also blocked by the G-protein inhibitor GDPβS and by protein tyrosine phosphatase (PTP) inhibitors such as bpV(phen) but is unaffected by serine/threonine kinase inhibitors (see Canepari & Ogden, 2003). The results indicate the involvement of a G-protein, protein tyrosine kinase/phosphatase (PTK/PTP), but exclude the PLC products IP_3 and diacylglycerol (DAG) in regulating the sEPSP. These ligands were therefore tested on the transient outward current in experiments where the pipette potential was held at −12 mV for more than 20 s prior to L-glutamate photorelease. Because of the run down of the outward current in cells incubated with AGA4A described above, the following protocol was applied to prevent spiking during pharmacological experiments. Slices were preincubated for 20–30 min with each test ligand or, in control, with no ligand. TTX (1 μM) and AGA4A (250 nM) were then applied and the sequence of photolytic L-glutamate applications was started 10 min after addition of AGA4A. Outward currents (measured at −12 mV) and inward currents (measured at −77 mV) were evoked by pulses of 30 or 60 μM photoreleased L-glutamate. The results are summarized in Fig. 2. Both early outward (shown at −12 mV) and

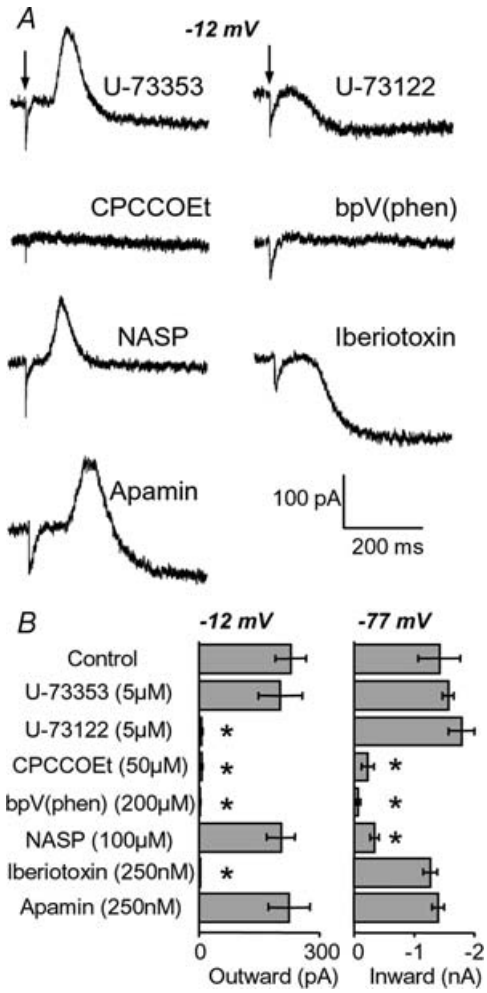

Figure 2. Pharmacology of mGluR1-mediated outward and inward currents evoked by photorelease of L-glutamate
A, mGluR1-mediated outward current evoked at −12 mV by photorelease of 30 μM L-glutamate after 20–30 min preincubation in the presence of the ligand indicated above each trace. *B*, bar graph of mean amplitude (± S.E.M.) of mGluR1-mediated outward current (left column, −12 mV) and inward current (right column, −77 mV) in five cells preincubated for 20–30 in the indicated ligand. After preincubation, each slice was incubated for 10 min in recording solution containing 100 μM NBQX, 50 μM AP5, 20 μM bicuculline, 1 μM TTX, 10 μM ZD-7288, 250 nM AGA4A and the test ligand at the indicated concentration. Note this protocol was used to avoid the run down of transient K^+ current seen in long exposures to AGA4A. Five control slices were preincubated for 20–30 min without ligand. Bicuculline was replaced by 100 μM picrotoxin when testing apamin and iberiotoxin. *Significant difference from control ($P < 0.01$, two population *t* test).

late inward (shown at −77 mV) currents were blocked by the mGluR1 antagonist CPCCOEt (50 μM), showing that activation of both conductances originates from mGluR1. The PLC inhibitor U73122 (5 μM) blocked the outward but not the inward current; control experiments with the inactive analogue U73353 (5 μM) showed no effect on either current under identical conditions. The BK Ca^{2+}-activated K^+ channel blocker iberiotoxin (250 nM) completely blocked the outward current but the SK blocker apamin (250 nM) was ineffective, indicating that the K^+ current is mediated by BK channels alone, although both are present in PNs. Neither toxin affected the slow inward current. These experiments used picrotoxin rather than bicuculline to block $GABA_A$ receptors. Evidence from Ca^{2+} imaging that the mGluR1-mediated transient outward current is activated by a transient rise of cytosolic free Ca^{2+} concentration is presented in detail below. Thus, the results support the idea that mGluR1 couples to two signalling pathways, and that the outward current is generated through BK channels gated by Ca^{2+} ions released from stores by IP_3 generated by PLC.

The tyrosine phosphatase inhibitor bpV(phen) (200 μM, Canepari & Ogden, 2003; see Posner *et al.* 1994) reversibly blocked both the transient outward current and the slow excitation, indicating that PTK/PTP regulation occurs at an early stage, before PLC activation; available evidence suggests that it is at the level of mGluR1 (Ireland *et al.* 2004) or the G-protein G_q (Umemori *et al.* 1999). The blocker of the mGluR1-mediated inward current, NA-spermine (100 μM), blocked the inward but not the outward mGluR1-mediated current, indicating that Ca^{2+} influx during an early phase of the mGluR1 excitatory conductance does not contribute to activation of the transient outward current. Together, the pharmacological results support divergence of the mGluR1 signalling pathway after the G-protein G_q (Hartmann *et al.* 2004) but before PLC, to generate a transient store-released cytosolic Ca^{2+} increase in one branch and a slow excitation (the sEPSP) and influx of Ca^{2+} through Ca^{2+}-permeable channels in the other.

Prior PN spiking or depolarization are required to prime the mGluR1-mediated outward current

In previous studies of PF-evoked, mGluR1-mediated slow excitation, trains of 4–10 stimuli at frequencies > 20 Hz were shown to evoke the sEPSC at −65 to −77 mV but showed no activation of an outward current (Canepari *et al.* 2004; Canepari & Ogden, 2003). Further experiments with PF stimulation in 300-μm thick coronal slices were conducted here to find the conditions that permit mGluR1-mediated activation of the transient outward current. PNs were allowed to fire spontaneously under current clamp to test their ability to prime the PLC-mediated response to tetanic PF stimulation in the molecular layer. The results for one cell are illustrated in Fig. 3. In control experiments, six pulses of PF stimulation at 200 Hz evoked inward sEPSCs that were > 100 pA in amplitude at −77 mV (Fig. 3*A*). To increase the driving potential for K^+ (in these experiments $E_K = -94$ mV), records were also obtained at −54 mV; here the sEPSC generated unclamped slow action currents due to limited space clamp and strong mGluR1-mediated excitation in the dendrites (Fig. 3*B*). Next, the cell was allowed to fire spontaneously for 20 s under current clamp (Fig. 3*C*, left trace) and then, after 500 ms, voltage clamped at −54 mV. In this case, PF stimulation evoked an outward current of 150 pA 100 ms after the end of the stimulation (top right trace in Fig. 3*C*). Both outward and inward currents were blocked by the mGluR1 antagonist CPCCOEt (50 μM, bottom right trace in Fig. 3*C*). In 12 cells tested first without and then with priming by prior spiking or depolarization, no outward current was detected at −77 or −54 mV without priming (detection limit, 10 pA). In contrast, outward current was seen in each cell following priming and averaged 78 pA (range, 20–160 pA) at −54 mV. The data are summarized in Fig. 3*D*. The sEPSC at −54 mV averaged −199 pA (range, −65 to −400 pA) without priming and −71 pA (range −20 to −180 pA) following priming. However, the reduced amplitude of sEPSC after priming may reflect residual depolarization in the dendrites. The priming protocol consisted either of a period of 2–20 s voltage clamped at −12 mV or firing under current clamp for 20 s. Spike firing under current clamp was with holding currents of 0 to −50 pA (mean, -37 ± 10 pA, $n = 15$) and periods of firing comprised bursts of fast, large amplitude spikes (mean 37% of the time) and slow spikes (mean 52% of the time) during priming.

Photorelease of L-glutamate instead of PF stimulation showed similar results in cells tested in both conditions. Figure 4*A* and *B* shows the excitatory current evoked in one cell by 30 μM L-glutamate at −77 and −53 mV, respectively. Figure 4*C* shows the generation of a transient outward current following a priming period of 20-s spiking under current clamp before testing under voltage clamp at −53 mV. Both the inward and outward currents evoked by photoreleased L-glutamate were blocked by addition of 50 μM CPCCOEt ($n = 3$ cells) indicating that both signals were due to mGluR1 activation. In five cells, no outward current was seen at −54 mV without priming, and in all cells the transient outward current was seen after priming (range, 90–310 pA). The data with and without priming are summarized in Fig. 4*D*. As noted above, in other experiments designed to investigate voltage dependence of the sEPSC, the outward current could be evoked by photoreleased L-glutamate without a formal priming protocol but only in cells held for long periods at −45 mV.

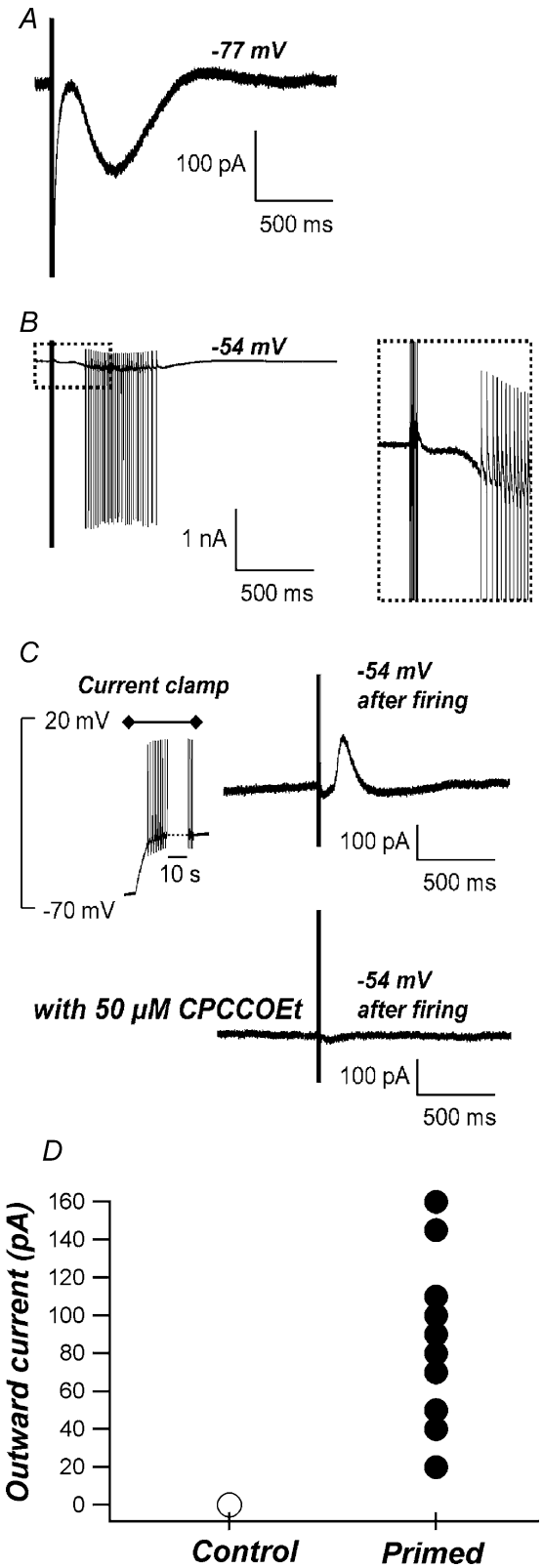

Figure 3. Transient outward current evoked by PF stimulation following spontaneous spiking
A, sEPSC at −77 mV evoked by a train of six pulses of PF stimulation at 200 Hz. *B*, same as *A* at −54 mV; unclamped action currents are associated with the sEPSC. Right panel shows an enlarged view of the region inside the dotted rectangle. *C*, current clamp recording, 20-s period of firing (left trace), followed 500 ms later by voltage clamp recording at −54 mV (upper right trace) showing the outward current evoked by six pulses of PF stimulation at 200 Hz; the same protocol was applied 10 min after the addition of 50 μM CPCCOEt (lower right trace). *D,* graph of amplitude of outward current from each cell without priming protocol (○, $n = 10$, no outward current detected) and following priming in the same cell by depolarization or spike firing (●). Symbol size is the peak-peak (p-p) noise, which is the detection limit of a transient current. External solution contained 50 μM NBQX. Holding currents at −54 mV averaged −37 ± 10 pA ($n = 15$).

Dependence of the mGluR1-activated conductances on PF stimulus parameters or L-glutamate concentration

The dependence of the transient outward and slow inward currents on the stimulus duration of the PF burst were compared in six cells in coronal slices by varying the number of pulses, usually at a frequency of 200 Hz. Figure 5*A* shows superimposed outward currents at −57 mV and inward sEPSCs at −77 mV evoked by two, three, four, six and eight stimuli at 200 Hz. Neither outward nor inward currents were seen with two pulses. However both increased in amplitude with three to six pulses. The outward current was maximal at four or six pulses, the inward current with six or eight pulses. The data from six cells are summarized in the bar graph of Fig. 5*B*. A difference in sensitivity was seen clearly in two cells where six pulses applied at 100 or 200 Hz showed maximal activation of the outward current at both frequencies but only submaximal activation of the inward sEPSC at 100 Hz. The results show that activation of the outward current requires shorter PF stimulation bursts than activation of the sEPSC and both are maximally activated by eight PF pulses at 200 Hz.

The amplitude and kinetics of transient outward current were investigated at four L-glutamate concentrations (6, 15, 30 and 60 μM) in 12 cells. To standardize the conditions for quantitative analysis, L-glutamate was photoreleased at −12 mV after depolarization for 20 s, within 15 min of adding TTX and AGA4A. Cable analysis with a two-compartment electrical model of each PN (see methods and Canepari *et al.* 2004), in the presence of the I_H inhibitor ZD-7288 (10 μM), gave an estimate of the dendritic membrane potential of -33 ± 0.57 mV ($n = 36$ cells) at 0.5–1.5 nA baseline current, at the time in the experimental protocol when L-glutamate was photoreleased. Figure 5*C* shows representative records of transient outward currents evoked in a PN at the four different L-glutamate concentrations. The outward current amplitude increased with the L-glutamate concentration from 6 μM and reached its maximal value at 30 μM. In the same cell, the mGluR1-mediated inward current at −77 mV increased further from 30 to 60 μM L-glutamate. In 12 cells, the mean

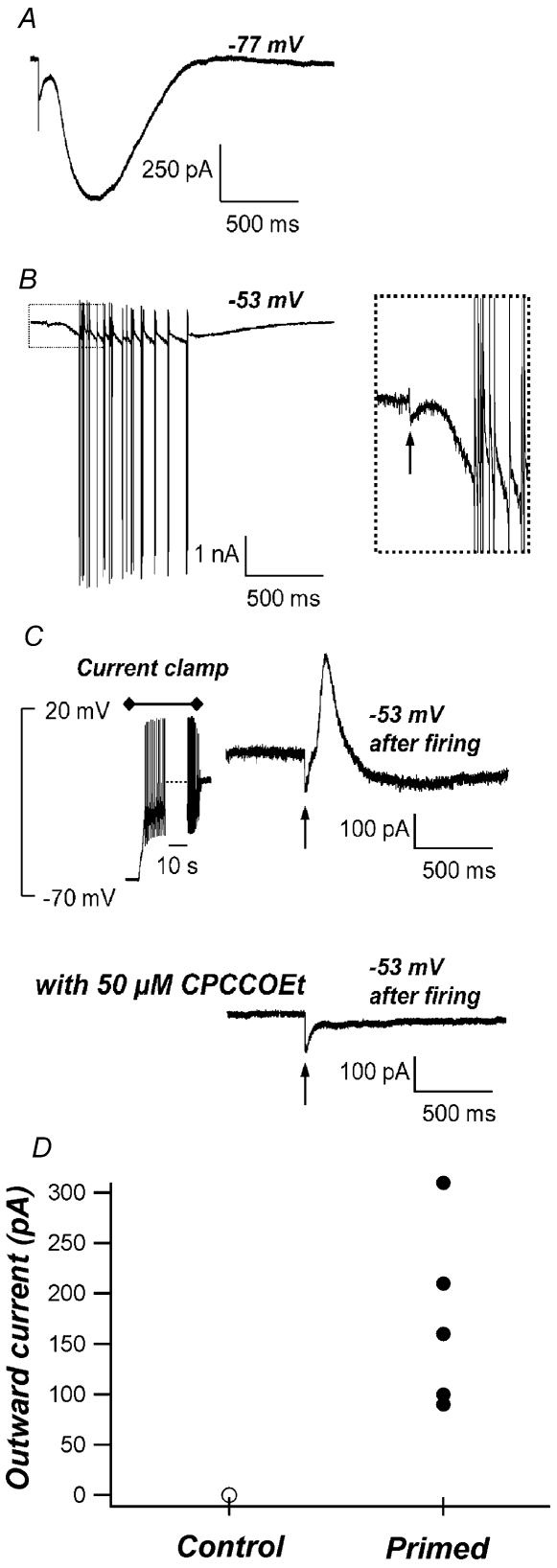

Figure 4. mGluR1-mediated currents evoked by photorelease of L-glutamate following spontaneous spiking
A, mGluR1-mediated inward current evoked at −77 mV by photorelease of 30 μM L-glutamate. *B*, photorelease of L-glutamate, as in *A*, at −53 mV activates the inward current with unclamped action currents but no outward current; region inside dotted rectangle is shown enlarged in right-hand panel. *C*, spontaneous firing under current clamp for 20 s (left trace) followed after 500 ms by voltage-clamp recording at −53 mV, showing the outward current evoked by photorelease of 30 μM L-glutamate (upper right trace). Lower right trace, same protocol applied 10 min after the addition of 50 μM CPCCOEt. *D,* graph of amplitude of outward current from each cell without priming (○, no detected current, $n = 5$) and following priming by depolarization or spike firing (●). Symbol size is the estimated resolution. External solution contained 50 μM NBQX.

outward currents at the four L-glutamate concentrations were 41.1 ± 11.6, 216.9 ± 41.2, 347.8 ± 51.4 and 350.1 ± 46.1 pA, respectively. The normalized amplitudes of transient outward and late inward mGluR1 currents at −12 and −77 mV are summarized in Fig. 5*D*. The results indicate that the outward current is activated at lower L-glutamate concentration than the inward current, although comparisons were not made at the same membrane potential and could be due to higher apparent affinity at more-positive potential. The outward current was fully activated by fewer PF stimulation pulses at 200 Hz and at lower L-glutamate concentrations than the inward current.

Precise timing and kinetics of the mGluR1-mediated outward current

The Ca^{2+}-dependent K^+ conductance in PNs was previously shown to be useful as a monitor of the kinetics of the underlying Ca^{2+} concentration following photolytic release of IP_3, or Ca^{2+} released directly from DM-nitrophen (Khodakhah & Ogden, 1995) and was used here to obtain kinetic information about the Ca^{2+} changes underlying the outward current. Inspection of the records in Fig. 5 shows that the transient outward current has a well-defined delay after activation by either PF stimulation or photoreleased L-glutamate, and that this is followed by rapid phases of activation and decline of the current. At 30 μM L-glutamate, the duration of the outward current transient measured at 50% amplitude was 85.2 ± 10.5 ms ($n = 12$ cells). The delay, measured as the time from the flash to the point where the amplitude increases above baseline, had an overall mean of 97.6 ± 14.3 ms ($n = 12$). However, the main interest is the reproducibility of the kinetics of the outward current in the same cell, as highly reproducible kinetics are unexpected in a multistep G-protein-coupled pathway and would indicate the presence of tight feedback regulation. The reproducibility in each PN was measured as the CV (S.D./mean) from five to eight consecutive responses at the same concentration in each cell. For the delay, the mean CV was $2.3 \pm 0.8\%$ ($n = 4$ cells) showing a small CV in each cell but also little cell–cell variability. The

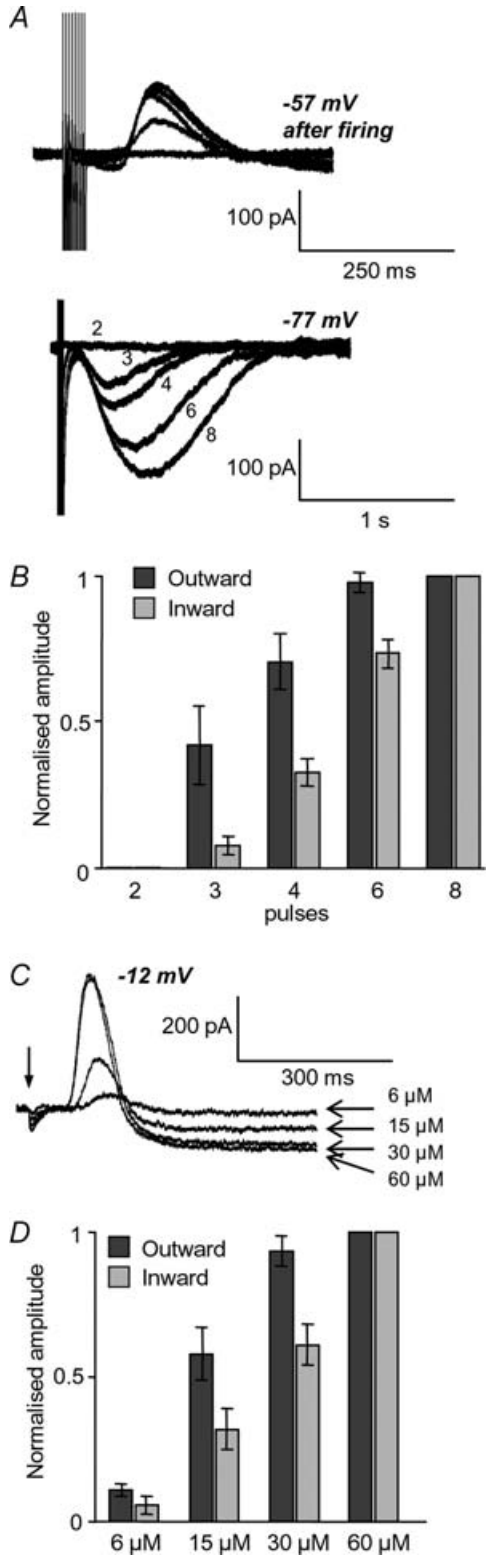

Figure 5. Dependence of mGluR1-mediated outward and inward currents on burst stimulation and L-glutamate concentration

A, 2–8 pulses of PF stimulation at 200 Hz. Upper traces show mGluR1-mediated outward current at −57 mV evoked 500 ms after spiking under current clamp for 10 s. Lower traces show sEPSC evoked at −77 mV; number of stimulation pulses indicated for each trace. Note different time scales in upper and lower traces. *B*, graph showing summary of mGluR1-mediated peak outward and peak inward current evoked by PF stimulation at 200 Hz normalized to the maximum at eight pulses; outward current at −50 to −60 mV after conditioning by spike firing or depolarization (−12 mV for 10 s; dark columns) and inward current (sEPSC) at −77 mV without conditioning (light columns). Data with two, three, four, six or eight pulses at 200 Hz, mean ± S.E.M. from six cells. *C*, mGluR1-mediated outward current evoked at −12 mV by photorelease of 6, 15, 30 or 60 μM L-glutamate. Arrow indicates time of flash. Recordings made after incubation for 10 min in the presence of 250 nM AGA4A. *D*, graph of peak mGluR1-mediated currents normalized to maximum at 60 μM L-glutamate; outward current (−12 mV; black columns) and inward current (−77 mV; grey columns) evoked by 6, 15, 30 or 60 μM L-glutamate; data from 12 cells (mean ± S.E.M). In *A* and *B* the solution contained 50 μM NBQX and in *C* and *D* 50 μM NBQX 1 μM TT_X and 250 nM AGA4A.

reproducibility of kinetics is illustrated by the superposition of traces in Fig. 6*A*. Similarly, the time from L-glutamate release (at 30 μM) to peak current from 12 cells was 148.8 ms ± 23.7, but the CV from five to eight consecutive responses in the same cell averaged 2.0 ± 0.8% ($n = 4$ cells). Both measurements show a very precisely timed interval, varying by approximately 2 ms in 100 ms, between mGluR1 activation and response in different trials in the same cell. Furthermore, the timing and kinetics of the outward current were only weakly dependent on L-glutamate concentration, the delay decreasing from a mean of 107.4 ± 15.6 ms ($n = 12$) at 15 μM to 91.5 ± 11.7 ms at 60 μM and the time to peak from 157.6 ± 25.5 ms ($n = 12$) at 15 μM to 136.6 ± 19.6 ms at 60 μM. Thus, although the amplitude of the outward current increased as concentration increased from 6 to 30 μM L-glutamate, the time course varied much less and was well defined within each PN. These results suggest that the kinetics of the mGluR1 activation pathway are tightly controlled by feedback, most probably cytosolic Ca^{2+} ions activating PLC (Okubo *et al.* 2004; Horowitz *et al.* 2005) and in a biphasic manner at the IP_3 receptor (Bezprozvanny *et al.* 1991; Finch *et al.* 1991). Furthermore, the constant kinetics with variable amplitude could be explained if individual units of Ca^{2+} release and K^+ channel activation were all-or-none because of feedback regulation and the amplitude were determined by the number of active units, possibly spines with different glutamate sensitivities, that respond in an all-or-none fashion as the stimulus increases.

Similar results were seen with PF stimulation. Over all cells, the delays measured from the first stimulus in bursts of six pulses at 200 Hz averaged 99.5 ± 4.2 ms ($n = 7$). However, consecutive outward currents evoked by PF stimulation in the same cell had a very precise timing, illustrated by the superimposed records shown in Fig. 6*B*. The CV of the delay and the time to peak from three or four consecutive responses within each cell averaged 1.9% and 3.5%, respectively. The possible roles of an accurately

timed interval between PF mGluR1 activation and Ca^{2+} release are discussed below.

Intracellular Ca^{2+} concentration changes associated with the mGluR1-mediated outward current

To test directly whether a delayed, fast-activating and -inactivating Ca^{2+} release into the cytosol underlies the mGluR1-mediated transient K^+ conductance, spatially uniform photorelease of L-glutamate was combined with fast Ca^{2+} imaging. A low-affinity indicator was used to minimize exogenous Ca^{2+} buffering that might distort the kinetics of Ca^{2+} release and detection. With 0.9 mM Oregon Green BAPTA-5N (dissociation constant, $K_{Ca} = 35\ \mu M$), Ca^{2+} buffering capacity due to the indicator calculated at a resting Ca^{2+} concentration of 50 nM is 26 bound/free, compared with the immobile buffering of 2000 estimated in PNs (Fierro & Llano, 1996). PNs were loaded for 30 min with the indicator and mGluR1 were activated by photorelease of 15, 30 or 60 μM L-glutamate after depolarizing to −12 mV for at least 20 s in the presence of TTX and AGA4A (applied 10 min before recording to minimize run down). A total of 400–1000 images at 50 Hz (exposure, 18.4 ms) were taken in subregions of the CCD, usually as strips of 512 × 32, 512 × 64 or 512 × 128 pixels orientated along the dendritic tree (512 pixels is 155 μm, 0.3 μm pixel^{-1}). To prevent CCD saturation by fluorescence originating in the soma, a 20% transmission neutral density (ND) filter covered one edge of the field and the CCD was moved on a rotating x–y stage to view the soma through the ND filter.

Figure 7*A* shows a fluorescence image of a PN with a highlighted strip of 155 μm × 39 μm for fast acquisition

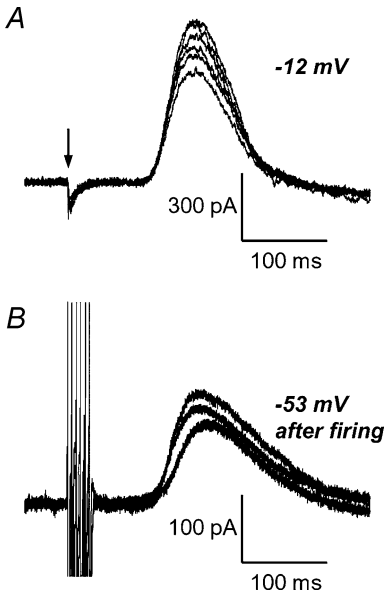

Figure 6. Reproducible timing and kinetics of the mGluR1-mediated outward current
A, superimposed outward currents evoked in the same PN by six consecutive pulses of 30 μM L-glutamate aligned to the time photorelease indicated by the arrow. −12 mV holding potential. External solution contained 100 μM NBQX, 50 μM AP5, 20 μM bicuculline, 1 μM TTX and 250 nM AGA4A. *B*, superimposed mGluR1-mediated outward currents at −53 mV from the same PN. Six pulses of PF stimulation at 200 Hz were aligned to the first stimulus. Each PF burst was applied 500 ms after firing for 10 s under current clamp. The solution contained 50 μM NBQX.

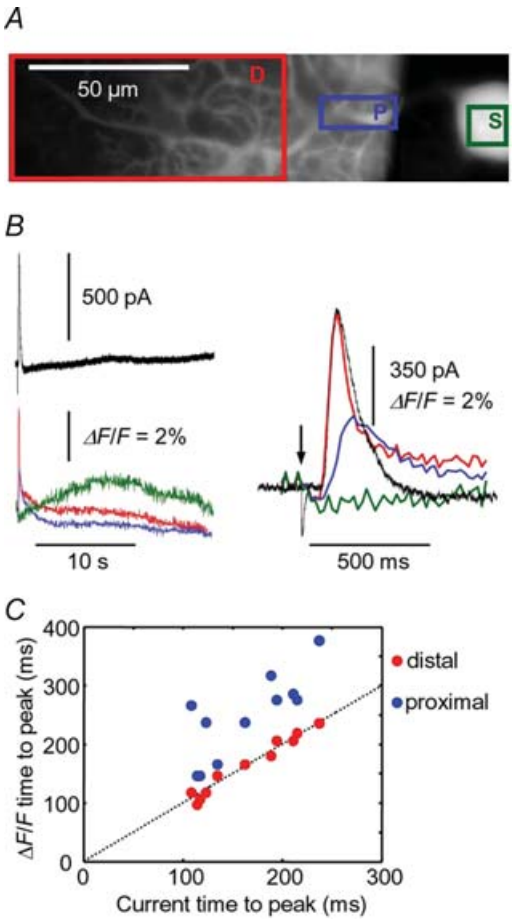

Figure 7. Changes in intracellular Ca^{2+} concentration associated with the mGluR1-mediated outward current
A, fluorescence image of a PN (average of 1000 frames, 512 pixels × 128 pixels) indicator 0.9 mM Oregon Green BAPTA-5N. Images acquired at 50 Hz (18.6 ms exposure); red, blue and green rectangles delimit the distal dendritic region (D, > 70 μM from the soma), the proximal region (P) and the soma (S), respectively. The soma is viewed through 20% transmission ND filter. *B*, upper-left, mGluR1-mediated outward current at −12 mV evoked by photorelease of 30 μM L-glutamate at the time indicated by the arrow (black trace); lower left, $\Delta F/F$ measured in the distal dendrite (red trace), proximal dendrite (blue trace) and soma (green trace); right-hand panel, $\Delta F/F$ records on a faster time scale and superimposed on the whole-cell current. Note that fluorescence after the flash is reduced by 0.2% by bleaching. *C*, time to peak of $\Delta F/F$ in the distal dendrites (●) and proximal dendrites (●) plotted against the time to peak of outward current G = 11 cells. Note that data from distal dendrites fall on the dotted line (slope = 1) for synchronous peaks of $\Delta F/F$ and K^+ current. External solution contained 100 μM NBQX, 50 μM AP5, 20 μM bicuculline, 1 μM TTX and 250 nM AGA4A.

and the soma covered by 20% ND filter. The PN image was divided into three rectangular regions corresponding to the soma (S, green), the proximal dendrite (P, blue) and the distal region > 70 μm from the soma (D, red). The time courses of the changes in $\Delta F/F$ in the three regions monitored at 50 Hz were compared with those of the transient outward current and the slow inward current. Figure 7*B* shows the mGluR1-mediated whole-cell current (black traces) evoked at −12 mV by photorelease of 30 μM L-glutamate on 10-s and 500-ms timescales for comparison with the time course of $\Delta F/F$ averaged within the three regions. The time course of $\Delta F/F$ in the distal region (red traces) peaked within the same 20 ms frame as the mGluR1-mediated outward current, whereas the $\Delta F/F$ in proximal dendites (blue) rose and fell substantially after the current, indicating that a large fraction of the K^+ current is activated by Ca^{2+} changes occurring in the distal region. In six cells in which somatic (green) $\Delta F/F$ measurements were obtained, three showed a slow $\Delta F/F$ of 1–3% in the soma, peaking at 3–8 s, as reported previously (Canepari *et al.* 2004).

The correlation between the Ca^{2+} increase and the outward current can be summarized as follows. In two cells, no changes in $\Delta F/F$ were detected in the distal or proximal subregions of the dendrite and these cells also showed no transient K^+ current following glutamate release. In a further five cells in which the peak transient K^+ current was less than 250 pA, the $\Delta F/F$ signal to noise ratio was too small to be reliable in showing the time course of the Ca^{2+} concentration changes. In a further 11 cells with large changes of $\Delta F/F$, the Ca^{2+} signal peaked in the distal before the proximal dendrites as in Fig. 7*B*. Peak transient outward current was greater than 250 pA in each of these cells. The temporal correlation of peak K^+ current with peak Ca^{2+} changes in the dendrites is summarized in Fig. 7*C*, which shows a graph of the time of the peak $\Delta F/F$ in the two regions against the time of the peak K^+ conductance (blue symbols, proximal region; red symbols, distal region). The dotted line has a slope of 1. The peak currents are best correlated with the peak $\Delta F/F$ in the distal dendritic regions, occurring in the same 20-ms time frame. The peak $\Delta F/F$ was delayed with respect to the peak K^+ current by a mean of 80.5 ± 17.3 ms ($n = 11$) in the proximal dendrite.

The K^+ current has been shown to follow closely the Ca^{2+} increase evoked by photoreleased IP_3 (Khodakhah & Ogden, 1995). The data obtained here indicate that the changes in Ca^{2+} concentration in the distal dendritic region are the main source of activation of the Ca^{2+}-activated K^+ conductance seen in whole-cell recording, and, furthermore, that the time course of the K^+ conductance evoked by photoreleased L-glutamate is similar to that of intracellular Ca^{2+} release in the distal region. The K^+ conductance evoked by PF stimulation, which will act at synapses on dendritic spines, has kinetics very similar to that evoked by photoreleased L-glutamate (compare Figs 5 and 6) further supporting the conclusion that the K^+ conductance due to photoreleased L-glutamate mainly reports Ca^{2+} changes close to PF–PN synapses.

Time-course of the Ca^{2+} change in subresolution structures below 1.5 μm

Advantage was taken of the planar morphology and small focal depth of PNs in sagittal slices used for imaging to compare the time course of Ca^{2+} changes occurring in spatially resolved dendrites with those in smaller, spatially unresolved structures which are less than 1.5 μm across. Spatial resolution is limited by the pixel size, measured as 0.3 μm square. Twenty regions of 32 × 32 pixels (9.7 × 9.7 μm) from 10 cells that had average $\Delta F/F$ greater than 10% were analysed with un-binned, 0.3-μm pixels as follows. The dendrites were identified using the Canny edge detection method, implemented in Matlab, that detects edges as local maxima of the gradient of the image after smoothing with a Gaussian filter (Canny, 1986). The results were visually tested against each fluorescence image and showed that structures bounded by edges separated by at least 1.5 μm (5 pixels) were reliably detected and were identified as small dendritic branches. The pixels within the two edges were grouped together as resolved structures. All remaining pixels were also grouped and corresponded to fluorescence originating in unresolved small structures (dendrites < 1.5 μm across and spines) and fluorescence originating in out-of-focus regions of the PN. The two groups of pixels in each subregion were analysed separately for $\Delta F/F$ to see which group, resolved or unresolved, responded earlier. An example of the procedure is shown in Fig. 8. Figure 8*A* shows the fluorescence image of a PN strip (512 × 32 pixels) and a region (32 × 32 pixels) in which pixels within structures larger than 1.5 μm are coded white and those smaller than 1.5 μm are coded black. $\Delta F/F$ in white and black pixels were analysed separately. Figure 8*B* shows the mGluR1-mediated outward current, and the $\Delta F/F$ in the white and black pixels on the same time scale. The $\Delta F/F$ in the black (unresolved) regions and in the white (resolved > 1.5 μm) regions in each 20-ms frame were plotted against frame number in time-register with the peak of the K^+ current (Fig. 8*C*). Although the peaks of all three occur within the same 20-ms period, it is apparent that the $\Delta F/F$ of the black unresolved structures rises and falls before that of the white regions. In this case normalizing both traces to the peak amplitude and subtracting the black from the white trace will yield a negative number on the rise and positive number on the fall. Formally, the difference between black and white pixels ($D_{B,W}$) at each time point (taken midway in each

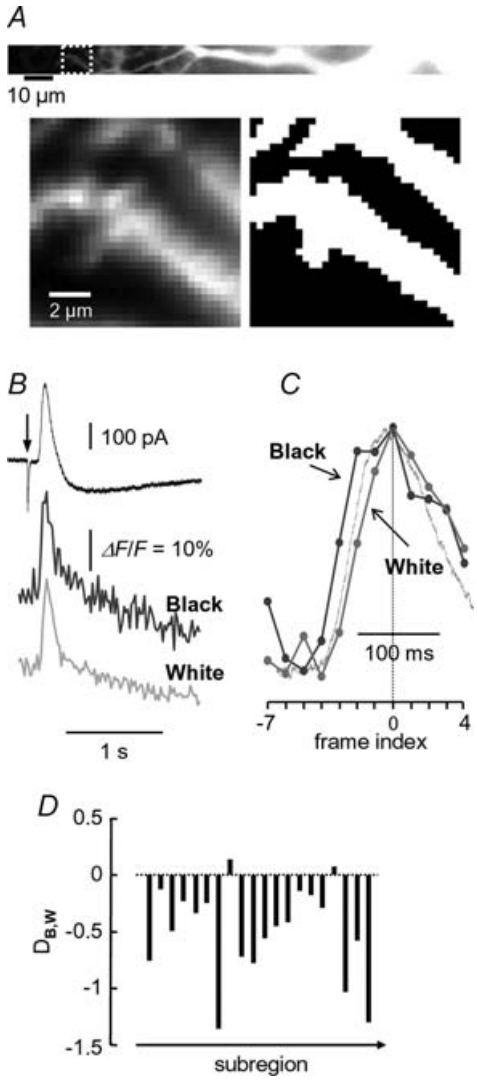

Figure 8. Time course of Ca^{2+} changes compared between resolved and unresolved dendritic structures
A, top, average of 400 taken at 50 Hz (18.6 ms exposure) in a strip of 155 μm × 9.7 μm (512 pixels × 32 pixels). PN filled with 0.9 mM Oregon Green BAPTA-5N; lower left, subregion (9.7 μm × 9.7 μm; 32 pixels × 32 pixels) indicated in the upper image bordered by the dotted white line; lower right, result of applying the Canny edge detection algorithm (see text) to the image on the left. Pixels coded white are contained within the edges of the resolved dendrite, while remaining pixels are coded black and represent non-fluorescent regions and fluorescence from un-resolved structures. *B*, upper trace, mGluR1-mediated outward current at −12 mV evoked by 30 μM L-glutamate (time of photorelease indicated by arrow); lower traces, $\Delta F/F$ of black pixels (dark grey trace) and of white pixels (light grey trace) of region shown in *A*. *C*, $\Delta F/F$ records of black and white pixels normalized to their maximal values and plotted against frame number (filled circles correspond to the mid-time of each frame); outward current is plotted on the same time scale (light grey trace). Dotted line is the mid-time of frame index 0 at $\Delta F/F$ peak. *D*, the difference of normalized $\Delta F/F$ of black minus white pixels at each time ($D_{B,W}$) calculated as described in the text (eqn (1)) is shown for 20 subregions of 32 pixels × 32 pixels with $\Delta F/F$ > 10% in 11 cells. Negative values show that $\Delta F/F$ changes in black pixels (unresolved structures) precede those in white pixels. External solution contained 100 μM NBQX, 50 μM AP5, 20 μM bicuculline, 1 μM TTX and 250 nM AGA4A.

frame) between the two sets of pixels was computed as:

$$D_{B,W} = \sum_{j=M-7}^{M+4} (N_B - N_W) \cdot \text{sign}(j - M) \qquad (1)$$

where N_B and N_W are the normalized $\Delta F/F$ of black and white pixels, respectively, j is the frame number, M is the frame number of the $\Delta F/F$ maximum of black pixels and 'sign($j-M$)' is 1 if $j > M$, 0 if $j = M$ and −1 if $j < M$. $D_{B,W}$ was computed over seven frames before the peak and four frames after and will be a negative number if the change in $\Delta F/F$ in the black pixels precedes that in white pixels. Figure 8*D* shows the values of $D_{B,W}$ computed for 20 regions of 9.7 μm × 9.7 μm from 10 cells. The values were large and negative in 18 out of 20 regions, showing that the changes in Ca^{2+} concentration in unresolved structures (less than 1.5 μm) preceded those in the visually identified small dendritic branches more than 1.5 μm across. The results indicate that with spatially uniform L-glutamate release the Ca^{2+} concentration change underlying the mGluR1-mediated outward current originated first in small structures less than 1.5 μm across, most probably spines (mean length 1.4 μm and diameter 0.45 μm in rat PN; Napper & Harvey, 1988). Spines will be present on resolved dendrites as well as in the unresolved regions indicating that the difference is likely to be underestimated by the analysis used here.

Kinetic separation of mGluR1-mediated Ca^{2+} concentration changes resulting from store release and influx

In small regions of the dendrites where Ca^{2+} signals from store release and influx were present together, a direct comparison could be made of the effect of priming on their time course and amplitude. Dendritic Ca^{2+} changes following photorelease of 30 μM L-glutamate at −12 mV were compared with those at −77 mV with or without a preceding 20-s depolarization to −12 mV to prime the response. At −77 mV, the driving potential for K^+ is small and Ca^{2+} sensitivity of BK channels low. Therefore, it is possible that the absence of an outward transient at negative potentials may reflect this. The effects of priming are illustrated in Fig. 9 for a distal subregion of 64 × 32 pixels of a PN (19.4 μm × 9.7 μm, Fig. 9*A*). This region had a large $\Delta F/F$ (approximately 30% peak) associated with the mGluR1-mediated outward current recorded at −12 mV (shown in the records of Fig. 9*B*). At −77 mV, both the outward current and large initial $\Delta F/F$ peak were absent, and a small, slow $\Delta F/F$ signal of 4% due to Ca^{2+} influx during the mGluR1-mediated inward current was seen (Fig. 9*C*; see Canepari *et al.* 2004). However, when the experiment was repeated at −77 mV after a 20-s depolarization to −12 mV, the early $\Delta F/F$ due to Ca^{2+} release from stores was restored, showing that the

early Ca^{2+} signal is present also at −77 mV after priming (Fig. 9*D*).The Ca^{2+} concentration transients are compared in Fig. 9*E* and show that the kinetics of the $\Delta F/F$ signals at −12 mV (trace b) and at −77 mV after a prepulse to −12 mV (trace c) were similar in amplitude and time course; both comprised an early peak and later slow component. The unprimed response (trace c) at −77 mV, due to Ca^{2+} influx via the sEPSC channel, can be subtracted from the primed response (trace d) to isolate the component due to priming. The resulting concentration difference shown in Fig. 9*F* (trace *d–c*) is transient; it rises and returns to baseline on the same time scale as the K^+ current at −12 mV, with a half-time of decline of 90 ms. It can be attributed to the store-released component of the primed Ca^{2+} change. Comparing the decline in half-time of the transient Ca^{2+} concentration determined in this way with that of the K^+ current gave mean values of 107 ± 12 ms and 101 ± 11 ms, respectively, in six cells. In contrast, the later small $\Delta F/F$ signal at −77 mV without priming was slower and followed the time course of the mGluR1-mediated inward current. Overall, the same results were seen in six out of six PNs tested in this way. Figure 9*G* summarizes the results by plotting the mean peak $\Delta F/F$ at −12 and −77 mV with and without priming. It shows large, early increases of $\Delta F/F$ of similar peak amplitudes in the responses at −12 mV and at −77 mV after pre-pulse to −12 mV that was absent without priming. The right hand panel shows the mean time to peak at −12 mV or at −77 mV, with or without the priming depolarization. The results distinguish the early, large Ca^{2+} peak in PNs following preconditioning depolarization

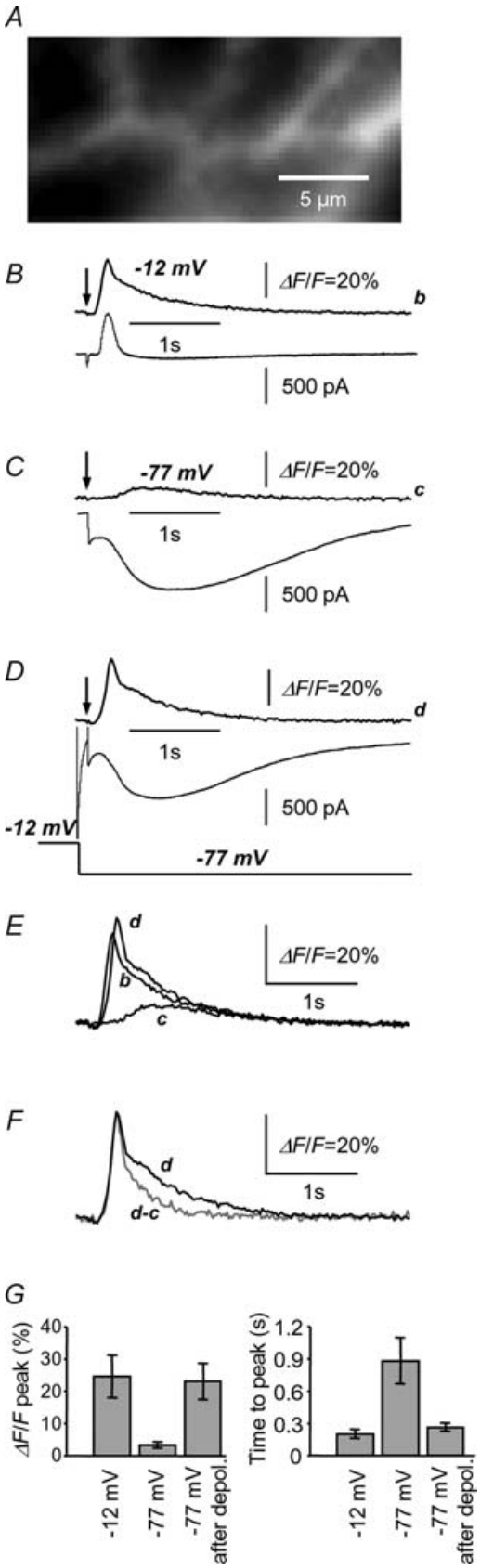

Figure 9. Kinetic separation of mGluR1-mediated intracellular Ca^{2+} changes arising from store release or influx
A, subregion (62 pixels × 32 pixels; 19.4 µm × 9.7 µm) from the fluorescence image of a PN filled with 0.9 mM Oregon Green BAPTA-5N. Average of 400 frames at 50 Hz (exposure, 18.6 ms). *B*, mGluR1-mediated current at −12 mV evoked by 30 µM L-glutamate (lower trace) and time course of $\Delta F/F$ averaged over the subregion shown in *A* (upper trace). *C*, mGluR1-mediated current at −77 mV evoked by 30 µM L-glutamate (lower trace) and time course of averaged $\Delta F/F$ over subregion shown in *A* (upper trace). *D*, mGluR1-mediated current at −77 mV evoked by photorelease of 30 µM L-glutamate 100 ms after a 20-s depolarization to −12 mV (lower trace) and $\Delta F/F$ in the subregion shown in *A* (upper trace). *E*, superimposed $\Delta F/F$ records shown in *B–D*. *F*, subtraction of the $\Delta F/F$ at −77 mV without depolarisation (trace *C* in panel *E*) from the $\Delta F/F$ in the same cell at −77 mV following depolarisation (trace *d*) is shown as trace *d-c* (grey). Note that trace of the difference has kinetics similar to that of the outward current. *G,* bar graph of $\Delta F/F$ peak amplitude following photorelease of 30 µM L-glutamate at −12 mV, −77 mV and at −77 mV after 20-s depolarization (left panel), and time to peak $\Delta F/F$ at −12 mV, −77 mV and at −77 mV after 20-s depolarization (right panel). Data are from six cells with outward current > 250 pA (−12 mV) and inward current < −1nA (−77 mV). Error bars indicate S.E.M. External solution contained 100 µM NBQX, 50 µM AP5, 20 µM bicuculline, 1 µM TTX and 250 nM AGA4A applied 10 min prior to flash.

from the relatively slow, small-amplitude Ca^{2+} change due to influx in the mGluR1-activated cation conductance. Thus the divergent mGluR1 pathways are sources of two kinetically distinct Ca^{2+} signals, one early, precisely timed transient change of large amplitude dependent on Ca^{2+} stores and the other a smaller amplitude, slower rising Ca^{2+} increase due to influx independent of Ca^{2+} stores.

Discussion

Two mGluR1-mediated signalling pathways

The results presented here show that activation of mGluR1 either by PF stimulation or by photorelease of L-glutamate evokes two ion conductances, a previously uncharacterized inhibitory transient K^+ conductance followed by a slow excitatory conductance (the sEPSC). The K^+ conductance is due to BK Ca^{2+}-activated channels, which are blocked by iberiotoxin but not apamin. It is sensitive to the PLCβ inhibitor U73122 (Cruzblanca *et al.* 1998; Haley *et al.* 2000; Horowitz *et al.* 2005) and has a time course that closely follows transient Ca^{2+} concentration changes measured in small dendritic structures, spines and small dendrites. In contrast, the sEPSC is a Ca^{2+}-permeable cation channel that produces a relatively small, slow Ca^{2+} increase by influx, and is insensitive to PLC inhibition. It is blocked by NASP and other drugs that block Ca^{2+}-permeable, unedited, non-NMDA GluR channels (Canepari *et al.* 2004). The K^+ conductance is insensitive to NASP and IEM1460, which block Ca^{2+} influx in the sEPSC channel, showing that there is no interdependence of the two pathways. Evidence from G-protein-deficient mice indicates that both pathways signal via Gq (Hartmann *et al.* 2004) and both were blocked by the tyrosine phosphatase inhibitor bpV(phen), indicating that the tyrosine phosphorylation/dephosphorylation shown previously to regulate the mGluR1-mediated sEPSC (Canepari & Ogden, 2003) acts at an early stage before the pathways diverge. The evidence available suggests that PTK/PTP may act at mGluR1 and G_q (Umemori *et al.* 1999; Ireland *et al.* 2004). The results therefore suggest a divergence at G_q, possibly with α_q activating PLCβ and $\beta\gamma$ activating the sEPSC pathway as suggested by Sugiyama *et al.* (1999). However, the two paths may be activated independently, in response to different conditions, and may occur in different subregions of the dendritic tree.

Glutamate sensitivity

The PLC-mediated pathway was elicited at lower L-glutamate concentrations and with shorter PF bursts than the sEPSC pathway. The relation between concentration and peak amplitude has an EC_{50} for L-glutamate of 1.5- to 2-fold higher for the sEPSC conductance than the early K^+ conductance. Comparable relative amplitudes were achieved with three pulses of PF stimulation at 200 Hz for the K^+ current and five pulses for the sEPSC.

Kinetics and comparison with IP_3-evoked Ca^{2+}release

The two membrane conductances and the associated Ca^{2+} concentration changes showed different kinetics. The outward current and the underlying transient Ca^{2+} increase peaked at 148 ± 24 ms after PF stimulation with a well-defined delay of 99.5 ± 4.2 ms. The sEPSC and associated Ca^{2+} influx peaked in 200–400 ms. These kinetics can be compared with the mGluR1-mediated Ca^{2+} changes evoked by local PF stimulation reported by Takechi *et al.* (1998) which showed an average initial delay of 198 ms before the Ca^{2+} rise and time to peak of 262 ms. The experimental conditions differ in the use here of Ca^{2+} priming protocols, a low-affinity Ca^{2+} indicator and the warmer temperature all of which may influence the time course, but there is also the possibility that store-release and influx were not well separated. No outward K^+ current was reported by Takechi *et al.* (1998) with local PF stimulation, nor by Finch & Augustine (1998), which showed local IP_3-evoked Ca^{2+} signals. However, the size of the K^+ current is relatively small and may not have been detected with local stimulation. The transient outward current is clearly seen following PF stimulation in PNs held at depolarized membrane potentials in the records of Galante & Diana (2004).

The K^+ conductance and Ca^{2+} concentration in the distal dendritic region showed surprisingly high precision in their delays and in the fast kinetics of the rise and fall. The difference from one response to the next in each PN measured as the CV was 1–2%, a 1–2 ms variation in the mean delay of 100 ms. Furthermore, the variation between cells was small and the delay and rise and fall of the Ca^{2+} concentration were little affected by L-glutamate concentration in the 15–60 μM range. This could be explained if PLC-mediated Ca^{2+} release occurs in an all-or-none manner with constant kinetics in many independent units and with the number of units recruited determining the amplitude. The fast all-or-none kinetics are consistent with signalling in the confined compartment of the spines of PF–PN synapses and suggests that the signalling cascade is tightly regulated, perhaps with colocalization of components of the PLC pathway as in *Drosophila* photoreceptors (Scott & Zuker, 1998). In support of this idea, the perisynaptic localization of PLCβ4 in PNs and co-immunoprecipitation with mGluR1α, IP_3 receptors and Homer scaffold protein has been described by Nakamura *et al.* (2004).

Ca^{2+} release from stores by IP_3 has been shown to activate a fast K^+ conductance in PNs with kinetics similar to the underlying Ca^{2+} change recorded simultaneously, which therefore provides a fast monitor of underlying free Ca^{2+} concentration (Khodakhah & Ogden, 1995). This

property and the kinetics of IP_3-evoked Ca^{2+} release are similar to the early outward current and underlying Ca^{2+} concentration changes reported here. mGluR1-mediated signalling via PLC requires several steps to produce Ca^{2+} release, including glutamate binding to mGluR1, receptor association with G_q, dissociation of α_q from $\beta\gamma$, phosphoinositide hydrolysis by PLCβ to IP_3 and DAG, IP_3 binding to receptors, Ca^{2+} flux and termination of Ca^{2+} release by Ca^{2+}-induced inactivation. Two points of feedback control have been identified in this signalling cascade: (i) the facilitatory action of Ca^{2+} at PLCβ (Okubo *et al.* 2004; Horowitz *et al.* 2005); and (ii) the effect of Ca^{2+} at the IP_3 receptor in facilitating activation and then in producing inactivation of Ca^{2+} flux as the Ca^{2+} concentration rises thus terminating Ca^{2+} release (Finch *et al.* 1991; Bezprozvanny *et al.* 1991; Ogden & Capiod, 1997). A facilitatory effect of prior Ca^{2+} influx on IP_3 receptors was not seen in PNs with photoreleased IP_3; however, it may be that facilitation at the IP_3 receptor requires Ca^{2+} influx after IP_3 release as reported in hippocampal neurones (Nakamura *et al.* 1999). Thus, the best-characterized positive, facilitatory interaction is between Ca^{2+} and PLCβ (Okubo *et al.* 2004; Horowitz *et al.* 2005). The subsequent negative regulation is the termination of Ca^{2+} flux from stores by accumulation of local high Ca^{2+} concentrations, which has been shown to be fast in PNs (Ogden & Capiod, 1997). The kinetic information available from photoreleased IP_3 in PNs can be compared with the kinetics of the transient, mGluR1-mediated, PLC-dependent Ca^{2+} release obtained here. Ca^{2+} release from stores in PNs has fast kinetics compared to peripheral tissues, with delays decreasing in the range of 10–50 ms with increasing IP_3 concentration. This is followed by a period of high Ca^{2+} flux for 10–50 ms, terminated by inactivation by a high local Ca^{2+} concentration, generating a rapid, transient Ca^{2+} concentration change. The duration of the Ca^{2+} flux judged by the rise-time of the K^+ conductance here is 40–50 ms, which is similar to that following photorelease of 20 μM IP_3 in the cytosol (Khodakhah & Ogden, 1995; Ogden & Capiod, 1997). The 100-ms delay before the rise of the K^+ conductance seen here, following PF stimulation or L-glutamate photorelease, is longer than that measured previously for the IP_3–Ca^{2+} release step at 20 μM IP_3, leaving a significant time (more than 50 ms) during which the initial interaction between mGluR1,G_q and PLCβ can occur. Recent fluorescence analysis has shown that the time course of G-protein-coupled receptor activation can be fast in some conditions (e.g. 40 ms for α2-adrenoceptor; Benians *et al.* 2005) and would be expedited by close apposition of signalling enzymes and substrates as reported in PN spines (Nakamura *et al.* 2004). The decline of the K^+ conductance was shown here to be similar to the decline of underlying free Ca^{2+} concentration. It will be affected by the high Ca^{2+} buffering capacity in PNs (estimated as 2000 : 1; Fierro & Llano, 1996) and the time course may be shaped by delayed buffering as a result of Mg^{2+}–Ca^{2+} exchange on parvalbumin, which is present at high concentrations in PNs (Kosaka *et al.* 1993). The rate of decline of Ca^{2+} concentration monitored by the Ca^{2+} indicator (see Fig. 9) or by the K^+ conductance, with half-times of 100 ms, is similar to the decline of Ca^{2+} transients in spines evoked by brief influx through voltage-gated channels (bi-exponential decays of 12 and 200 ms, Schmidt *et al.* 2003). This is faster than the decline in larger dendrites or the soma and further supports the idea that the PLC-dependent signalling occurs mainly in small dendritic structures such as spines.

Location of PLC-dependent signals

The location of the increase of free Ca^{2+} concentration underlying the K^+ conductance seen here was identified by comparing the time course of the Ca^{2+} concentration change in different regions with the whole-cell current elicited by spatially uniform L-glutamate photorelease. The results showed that the Ca^{2+} increase underlying the K^+ conductance was mainly in the distal dendritic region. There was little contribution from proximal regions, where Ca^{2+} changes were delayed by 80 ms with respect to the peak K^+ current, or from somatic changes, which were delayed by several seconds. To obtain more detail of the location of the PLC-dependent Ca^{2+} change, the time course of Ca^{2+} changes following L-glutamate photorelease in dendrites larger than 1.5 μm was compared with adjacent, spatially unresolved smaller structures less than 1.5 μm across. This indicated that the Ca^{2+} concentration rises first in small structures adjacent to dendritic branches, most probably spines of PN synapses. This is also supported by the similar delays and kinetics of the K^+ conductance, whether elicited by uniform L-glutamate photorelease or synaptically by PF stimulation, and by the similar fast kinetics of Ca^{2+} here to that seen previously in spines as discussed above (Schmidt *et al.* 2003).

The K^+ current was blocked by iberiotoxin but not by apamin, indicating Ca^{2+}-dependent activation of BK but not SK channels, although both are expressed in PNs (Womack & Khodakhah, 2002*a*; Cingolani *et al.* 2002; Edgerton & Reinhart, 2003). This suggests that only BK channels are associated with the sites of mGluR1-mediated store-released Ca^{2+}.

The requirement for PN activity prior to mGluR1-mediated transient Ca^{2+} release

The fast intracellular Ca^{2+} release and the associated K^+ current activated by mGluR1 were not seen previously with PF stimulation or photoreleased L-glutamate in experiments in quiescent PNs. The results here show a requirement for prior electrical activity, either spiking or depolarization. In the presence of AGA4A, the transient

Ca^{2+} release and K^+ current showed run down increasing with duration of exposure as AGA4A progressively inhibited the Ca^{2+} conductance. This suggests a role of Ca^{2+} influx through P/Q-type Ca^{2+} channels in the priming process. The priming by spontaneous spiking of PNs was evoked with small, steady current injections (0 to −50 pA). Spikes occurred at frequencies observed in non-invasive extracellular recordings (Womack & Khodakhah, 2002*b*) and showed bursts of fast and slow rising spikes. Although fast spikes are reported not to invade the dendrites (Stuart & Hausser, 1994), dendritic conductances are known to influence PN firing modes, indicating that there is spread of fast spike potential into the dendrites and that this may activate Ca^{2+} influx (Womack & Khodakhah, 2002*b*). It would be interesting to know whether CF-evoked complex spikes, which generate dendritic Ca^{2+} spikes, are effective in priming the response. However, these experiments are not possible with the present protocol because of the need to block ionotropic L-glutamate receptors in photorelease experiments described here.

A clear requirement for 'priming' by Ca^{2+} influx through voltage-gated channels has been described recently in pyramidal neurones of basolateral amygdala (Power & Sah, 2005). This was attributed to store-filling, tested by photorelease of IP_3. This does not appear to be the mechanism here. IP_3 photoreleased in quiescent PNs is effective in releasing Ca^{2+} from stores, although it should be noted that high concentrations are required (Khodakhah & Ogden, 1993, 1995). Re-examinantion of the data confirms that priming protocols similar to those required for activation of the PLC-dependent mGluR1-mediated release from stores were not required to see IP_3-evoked Ca^{2+} release. The present experiments do not directly distinguish between contributions to the priming from store filling and from a facilitatory effect of Ca^{2+} on PLCβ or on IP_3 receptors. Previous experiments showed that elevation of the Ca^{2+} concentration to micromolar levels 100 ms prior to IP_3 release strongly inhibited Ca^{2+} flux from stores, and lower levels of Ca^{2+} elevation showed no potentiation at $InsP_3$ receptors (Khodakhah & Ogden, 1995; Ogden & Capiod, 1997). The ability of photoreleased IP_3 to release Ca^{2+} in quiescent PNs and the known sensitivity of PLCβ in PNs to elevated cytosolic Ca^{2+} concentration (Okubo *et al.* 2004; Horowitz *et al.* 2005) therefore suggest that potentiation of PLC β by Ca^{2+} influx is the more likely. Experiments to examine the Ca^{2+} concentration in priming will require measurement protocols different from those used here, with high affinity indicators to measure small priming levels of Ca^{2+}.

Physiological role of K^+ conductance

The K^+ current was used here as a monitor of the kinetics of the underlying Ca^{2+} changes but its role in excitability should be considered. Generally, the K^+ conductance was small relative to other membrane conductances evoked during synaptic transmission in PNs, and the resulting small decline in excitability does not have an obvious role. However, it is possible that the local Ca^{2+} rise generates sufficient K^+ conductance to repolarise dendritic regions that receive burst input from PFs. Also, it may contribute in the dendrites to termination of bursts of fast spiking (Womack & Khodakhah, 2002*b*) or to resetting the down level of the bi-stable membrane potential of PNs (Loewenstein *et al.* 2005).

Interactions with other inputs

The precision of the delay between PF tetanic stimulation and Ca^{2+} release from stores via mGluR1-mediated phosphoinositide signalling may be important in the timing of interactions with other inputs, particularly CF inputs in PF synaptic plasticity. PF LTD is thought to be due to AMPA receptor internalization following phosphorylation by the combined activation of protein kinase C (PKC, Linden & Connor, 1991; de Zeeuw *et al.* 1998) and inhibition of protein phosphatase 2A (PP-2A, Launey *et al.* 2004). PKC is activated by mGluR1 via PLC, requiring Ca^{2+} and DAG, and PP-2A inhibition is the final step of a cascade involving guanylyl cyclase, cGMP, protein kinase G and G-substrate. This signalling cascade is initiated by NO release from PF terminals following presynaptic NMDA receptor activation (Casado *et al.* 2000, 2002; for review see Hartell, 2001). CF stimulation to generate a complex spike and Ca^{2+} influx during the 100 ms delay of the PF mGluR1 response, will result in additional Ca^{2+} that may facilitate activation of PLC β (Okubo *et al.* 2004), thus generating DAG, and may interact cooperatively with IP_3-bound IP_3 receptors to facilitate Ca^{2+} release (Nakamura *et al.* 1999; Wang *et al.* 2000). The timing may be important because of the strong inhibitory effect of prior Ca^{2+} influx on IP_3-evoked release seen in PNs (Khodakhah & Ogden, 1995; Ogden & Capiod, 1997). It has been reported that the timing of the CF input 150 ms after PF bursts is optimal for induction of LTD (Chen & Thompson, 1995) and for the supralinear summation of Ca^{2+} changes (Wang *et al.* 2000) including those underlying endocanabinoid release from PN dendrites (Brenowitz & Regehr, 2005).

References

Aiba A, Kano M, Chen C, Stanton ME, Fox GD, Herrup K, Zwingman TA & Tonegawa S (1994). Deficient cerebellar long-term depression and impaired motor learning in mGluR1 mutant mice. *Cell* **79**, 377–388.

Batchelor AM, Madge DJ & Garthwaite J (1994). Synaptic activation of metabotropic glutamate receptors in the parallel fibre-Purkinje cell pathway in rat cerebellar slices. *Neuroscience* **63**, 911–915.

Baude A, Nusser Z, Roberts JD, Mulvihill E, McIlhinney RA & Somogyi P (1993). The metabotropic glutamate receptor (mGluR1 alpha) is concentrated at perisynaptic membrane of neuronal subpopulations as detected by immunogold reaction. *Neuron* **11**, 771–787.

Benians A, Nobles M, Hosny S & Tinker A (2005). Regulators of G-protein signaling form a quarternary complex with the agonist, receptor and G-protein. A novel explanation for the acceleration of the signalling activation kinetics. *J Biol Chem* **280**, 13383–13394.

Bezprozvanny I, Watras J & Ehrlich BE (1991). Bell-shaped calcium-response curves of Ins (1,4,5)-trisphosophate and calcium-gated channels from endoplasmic reticulum of cerebellum. *Nature* **351**, 751–754.

Brenowitz SD & Regehr WD (2005). Associative short-term synaptic plasticity mediated by endocannabinoids. *Neuron* **45**, 419–431.

Canepari M, Auger C & Ogden D (2004). Ca^{2+} ion permeability and single-channel properties of the metabotropic slow EPSC of rat Purkinje neurons. *J Neurosci* **24**, 3563–3573.

Canepari M, Nelson L, Papageorgiou G, Corrie JET & Ogden D (2001*a*). Photochemical and pharmacological evaluation of 7-nitroindolinyl- and 4-methoxy-7-nitroindolinyl-amino acids as novel, fast caged neurotransmitters. *J Neurosci Methods* **112**, 29–42.

Canepari M & Ogden D (2003). Evidence for protein tyrosine phosphatase, tyrosine kinase, and G-protein regulation of the parallel fiber metabotropic slow EPSC of rat cerebellar Purkinje neurons. *J Neurosci* **23**, 4066–4071.

Canepari M, Papageorgiou G, Corrie JET, Watkins C & Ogden D (2001*b*). The conductance underlying the parallel fibre slow EPSP in rat cerebellar Purkinje neurones studied with photolytic release of L-glutamate. *J Physiol* **533**, 765–772.

Canny J (1986). A Computational Approach to Edge Detection. *IEEE Trans Pattern Anal Mach Intell* ***PAMI*-8**, 679–698.

Casado M, Dieudonne S & Ascher P (2000). Presynaptic N-methyl-D-aspartate receptors at the parallel fiber-Purkinje cell synapse. *Proc Natl Acad Sci U S A* **97**, 11593–11597.

Casado M, Isope P & Ascher P (2002). Involvement of presynaptic N-methyl-D-aspartate receptors in cerebellar long-term depression. *Neuron* **33**, 123–130.

Chen C & Thompson RF (1995). Temporal specificity of long-term depression in parallel fiber-Purkinje synapses in rat cerebellar slice. *Learn Mem* **2**, 185–198.

Cingolani LA, Gymnopoulos M, Boccaccio A, Stocker M & Pedarzani P (2002). Developmental regulation of small-conductance Ca^{2+}-activated K^+ channel expression and function in rat Purkinje neurons. *J Neurosci* **22**, 4456–4467.

Coesmans M, Smitt PA, Linden DJ, Shigemoto R, Hirano T, Yamakawa Y *et al.* (2003). Mechanisms underlying cerebellar motor deficits due to mGluR1-autoantibodies. *Ann Neurol* **53**, 325–336.

Conquet F, Bashir ZI, Davies CH, Daniel H, Ferraguti F, Bordi F *et al.* (1994). Motor deficit and impairment of synaptic plasticity in mice lacking mGluR1. *Nature* **372**, 237–243.

Cruzblanca H, Koh DS & Hille B (1998). Bradykinin inhibits M current via phospholipase C and Ca^{2+} release from IP3-sensitive Ca^{2+} stores in rat sympathetic neurons. *Proc Natl Acad Sci U S A* **95**, 7151–7156.

Daniel H, Levenes C, Fagni L, Conquet F, Bockaert J & Crepel F (1999). Inositol-1,4,5-trisphosphate-mediated rescue of cerebellar long-term depression in subtype 1 metabotropic glutamate receptor mutant mouse. *Neuroscience* **92**, 1–6.

De Zeeuw CI, Hansel C, Bian F, Koekkoek SK, van Alphen AM, Linden DJ & Oberdick J (1998). Expression of a protein kinase C inhibitor in Purkinje cells blocks cerebellar LTD and adaptation of the vestibulo-ocular reflex. *Neuron* **20**, 495–508.

DiGregorio DA & Vergara JL (1997). Localized detection of action potential-induced presynaptic calcium transients at a Xenopus neuromuscular junction. *J Physiol* **505**, 585–592.

Doroshenko PA, Woppmann A, Miljanich G & Augustine GJ (1997). Pharmacologically distinct presynaptic calcium channels in cerebellar excitatory and inhibitory synapses. *Neuropharmacology* **36**, 865–872.

Edgerton JR & Reinhart PH (2003). Distinct contributions of small and large conductance Ca^{2+}-activated K^+ channels to rat Purkinje neuron function. *J Physiol* **548**, 53–69.

Fierro L & Llano I (1996). High endogenous calcium buffering in Purkinje cells from rat cerebellar slices. *J Physiol* **496**, 617–625.

Finch EA & Augustine GJ (1998). Local calcium signalling by inositol-1,4,5-trisphosphate in Purkinje cell dendrites. *Nature* **396**, 753–756.

Finch EA, Turner TJ & Goldin SM (1991). Calcium as a coagonist of inositol-1,4,5-trisphosphate-induced calcium release. *Science* **252**, 443–446.

Fujiwara A, Hirose K, Yamazawa T & Iino M (2001). Reduced IP3 sensitivity of IP3 receptor in Purkinje neurons. *Neuroreport* **12**, 2647–2651.

Galante M & Diana M (2004). Group I metabotropic glutamate receptors inhibit GABA release at interneuron-Purkinje cell synapses through endocannabinoid production. *J Neurosci* **24**, 4865–4874.

Haley JE, Abogadie FC, Fernandez-Fernandez JM, Dayrell M, Vallis Y, Buckley NJ & Brown DA (2000). Bradykinin, but not muscarinic, inhibition of M-current in rat sympathetic ganglion neurons involves phospholipase C-beta 4. *J Neurosci* **20**, RC105.

Hartell NA (2001). Receptors, second messengers and protein kinases required for heterosynaptic cerebellar long-term depression. *Neuropharmacology* **40**, 148–161.

Hartmann J, Blum R, Kovalchuk Y, Adelsberger H, Kuner R, Durand GM, Miyata M, Kano M, Offermanns S & Konnerth A (2004). Distinct roles of $G_{\alpha q}$ and G_{11} for Purkinje cell signalling and motor behavior. *J Neurosci* **24**, 5119–5130.

Horowitz LF, Hirdes W, Suh BC, Hilgemann DW, Mackie K & Hille B (2005). Phospholipase C in living cells: activation, inhibition, Ca^{2+} requirement and regulation of M current. *J Gen Physiol* **126**, 243–262.

Ichise T, Kano M, Hashimoto K, Yanagihara D, Nakao K, Shigemoto R, Katsuki M & Aiba A (2000). mGluR1 in cerebellar Purkinje cells essential for long-term depression, synapse elimination, and motor coordination. *Science* **288**, 1832–1835.

Ireland DR, Guevremont D, Williams JM & Abraham WC (2004). Metabotropic glutamate receptor-mediated depression of the slow afterhyperpolarization is gated by tyrosine phosphatases in hippocampal CA1 pyramidal neurons. *J Neurophysiol* **92**, 2811–2819.

Khodakhah K & Armstrong CM (1997). Induction of long-term depression and rebound potentiation by inositol trisphosphate in cerebellar Purkinje neurons. *Proc Natl Acad Sci U S A* **94**, 14009–14014.

Khodakhah K & Ogden D (1993). Functional heterogeneity of calcium release by inositol trisphosphate in single Purkinje neurones, cultured cerebellar astrocytes, and peripheral tissues. *Proc Natl Acad Sci U S A* **90**, 4976–4980.

Khodakhah K & Ogden D (1995). Fast activation and inactivation of inositol trisphosphate-evoked Ca^{2+} release in rat cerebellar Purkinje neurones. *J Physiol* **487**, 343–358.

Kim SJ, Kim YS, Yuan JP, Petralia RS, Worley PF & Linden DJ (2003). Activation of the TRPC1 cation channel by metabotropic glutamate receptor mGluR1. *Nature* **426**, 285–291.

Kishimoto Y, Fujimichi R, Araishi K, Kawahara S, Kano M, Aiba A & Kirino Y (2002). mGluR1 in cerebellar Purkinje cells is required for normal association of temporally contiguous stimuli in classical conditioning. *Eur J Neurosci* **16**, 2416–2424.

Kosaka T, Kosaka K, Nakayama T, Hunziker W & Heizmann CW (1993). Axons and axon terminals of cerebellar Purkinje cells and basket cells have higher levels of parvalbumin immunoreactivity than somata and dendrites: quantitative analysis by immunogold labeling. *Exp Brain Res* **93**, 483–491.

Launey T, Endo S, Sakai R, Harano J & Ito M (2004). Protein phosphatase 2A inhibition induces cerebellar long-term depression and declustering of synaptic AMPA receptor. *Proc Natl Acad Sci U S A* **101**, 676–681.

Linden DJ & Connor JA (1991). Participation of postsynaptic PKC in cerebellar long-term depression in culture. *Science* **254**, 1656–1659.

Loewenstein Y, Mahon S, Chadderton P, Kitamura K, Sompolinsky H, Yarom Y & Hausser M (2005). Bistability of cerebellar Purkinje cells modulated by sensory stimulation. *Nat Neurosci* **8**, 202–211.

Mauk MD, Garcia KS, Medina JF & Steele PM (1998). Does cerebellar LTD mediate motor learning? Toward a resolution without a smoking gun. *Neuron* **20**, 359–362.

Nakamura M, Sato K, Fukaya M, Araishi K, Aiba A, Kano M & Watanabe M (2004). Signalling complex formation of phospholipase Cβ4 with metabotropic glutamate receptor 1α and inositol 1,4,5-trisphosphate receptor at the perisynapse and endoplasmic reticulum in mouse brain. *Eur J Neurosci* **20**, 2929–2944.

Nakamura T, Barbara JG, Nakamura K & Ross WN (1999). Synergistic release of Ca^{2+} from IP_3-sensitive stores evoked by synaptic activation of mGluRs paired with backpropagating action potentials. *Neuron* **24**, 727–737.

Napper RM & Harvey RJ (1988). Quantitative study of the Purkinje cell dendritic spines in the rat cerebellum. *J Comp Neurol* **274**, 158–167.

Ogden D (1996). Intracellular calcium release in central neurones. *Seminars in the Neurosciences* **8**(5), 281–291.

Ogden D & Capiod T (1997). Regulation of Ca^{2+} release by IP_3 in single guinea pig hepatocytes and rat Purkinje neurons. *J Gen Physiol* **109**, 741–756.

Okubo Y, Kakizawa S, Hirose K & Iino M (2004). Cross talk between metabotropic and ionotropic glutamate receptor-mediated signaling in parallel fiber-induced inositol-1,4,5-trisphosphate production in cerebellar Purkinje cells. *J Neurosci* **24**, 9513–9520.

Papageorgiou G, Ogden D, Barth A & Corrie JET (1999). Photorelease of carboxylic acids from 1-acyl-7-nitroindolines in aqueous solution: rapid and efficient photorelease of L-glutamate. *J Am Chem Soc* **121**, 6503–6504.

Posner BI, Faure R, Burgess JW, Bevan AP, Lachance D, Zhang-Sun G, Fantus G, Ng JB, Hall DA, Lum BS & Shaver A (1994). Peroxovanadium compounds. A new class of potent phosphotyrosine phosphatase inhibitors which are insulin mimetics. *J Biol Chem* **269**, 4596–4604.

Power JM & Sah P (2005). Intracellular calcium store filling by an L-type calcium current in the basolateral amygdala at subthreshold membrane potentials. *J Physiol* **562**, 439–453.

Schmidt H, Stiefel KM, Racay P, Schwaller B & Eilers J (2003). Mutational analysis of dendritic Ca^{2+} kinetics in rodent Purkinje cells: role of parvalbumin and calbindin D28k. *J Physiol* **551**, 13–32.

Scott K & Zuker CS (1998). Assembly of the Drosophila phototransduction cascade into a signalling complex shapes elementary responses. *Nature* **395**, 805–808.

Sillevis-Smitt P, Kinoshita A, De Leeuw B, Moll W, Coesmans M, Jaarsma D *et al.* (2000). Paraneoplastic cerebellar ataxia due to autoantibodies against a glutamate receptor. *N Engl J Med* **342**, 21–27.

Stuart G & Hausser M (1994). Initiation and spread of sodium action potentials in cerebellar Purkinje neurons. *Neuron* **13**, 703–712.

Sugiyama T, Hirono M, Suzuki K, Nakamura Y, Aiba A, Nakamura K, Nakao K, Katsuki M & Yoshioka T (1999). Localization of phospholipase C beta isozymes in the mouse cerebellum. *Biochem Biophys Res Commun* **265**, 473–478.

Takechi H, Eilers J & Konnerth A (1998). A new class of synaptic response involving calcium release in dendritic spines. *Nature* **396**, 757–760.

Umemori H, Hayashi T, Inoue T, Nakanishi S, Mikoshiba K & Yamamoto T (1999). Involvement of protein tyrosine phosphatases in activation of the trimeric G protein Gq/11. *Oncogene* **18**, 7399–7402.

Wang SS, Denk W & Häusser M (2000). Coincidence detection in single dendritic spines mediated by calcium release. *Nat Neurosci* **3**, 1266–1273.

Womack MD & Khodakhah K (2002*a*). Characterization of large conductance Ca^{2+}-activated K^+ channels in cerebellar Purkinje neurons. *Eur J Neurosci* **16**, 1214–1222.

Womack MD & Khodakhah K (2002*b*). Active contribution of dendrites to the tonic and trimodal patterns of activity in cerebellar Purkinje neurons. *J Neurosci* **22**, 10603–10612.

Acknowledgements

We thank John Corrie and George Papageorgiou (National Institute for Medical Research, London, UK) for providing MNI-caged L-glutamate and for advice and discussion, Kamran Khodakhah for discussion and Céline Auger, Alain Marty and John Corrie for comments on the manuscript. This work was supported by the Medical Research Council.